GEOPHYSICAL RESEARCH LETTERS, VOL. 21, NO. 24, PAGES 2613-2616, DECEMBER 1, 1994

Frequency dependence of the visibility and depths of mantle seismic discontinuities

George Helffrich[1] and Craig R. Bina[2]

Abstract. The visibility and apparent position of a seismic gradient zone depends on the seismic wave frequency at which it is observed, which we illustrate by showing how the visibility and depth of the olivine $\alpha \rightarrow \beta$ phase transformation (410 km discontinuity) change as temperature varies. Temperature variations change bottomside reflection coefficients by factors of 2-4 in the 0.5-1.0 Hz frequency band, which can explain spatial variability in short period $P'_{410}P'$ observations and the small apparent variability in observed 410 km discontinuity depths. Discontinuity depths inferred from the time lags of these reflections are also frequency dependent, leading to a frequency dependence of estimates of mantle lateral thermal variability based on discontinuity displacements. The frequency dependent seismic Clapeyron slopes for the olivine $\alpha \rightarrow \beta$ phase change we compute are 2.04 MPa K^{-1} at 0.2 Hz and 2.12 MPa K^{-1} at 0.05 Hz, and differ significantly from thermodynamic slope for the Mg_2SiO_4 end-member.

Introduction

It is generally accepted that phase transformations in mantle mineralogies demark the major seismic discontinuities within in the earth at 410 and 660 kilometers depth. Historically, one of the principal objections to this view was that the transformations progressed through too broad a depth interval to make them visible to seismic waves, but the phase change hypothesis has continued to find support in improved thermodynamic constraints on the transformations [Bina and Wood, 1987; Katsura and Ito, 1989; Fei et al., 1991]. Nevertheless, product and reactant phases do coexist within a transition region, yielding finite velocity gradients. Given the discontinuities' visibility to short period seismic waves, the gradients must be steep.

Richards [1972] explored a range of plausible profiles through gradient zones, showing that their ability to reflect and interconvert P and S waves depends on a seismic wave's frequency, or equivalently, wavelength. Short period visibility imposes severe constraints on velocity gradients; 1.0-1.5 Hz reflections from the 410 necessitate gradient thicknesses $\leq$ 4 km [Benz and Vidale, 1993]. Other frequency dependent properties arise however, which we identify here and explore. Since these effects stem from the way that the thermodynamic parameters influence the phase distribution through a transition, we begin with an examination of this dependence.

Thermodynamic Controls on Velocity Gradients

The Clapeyron (P-T) slope of a univariant reaction, $\frac{dP}{dT} = \frac{\Delta S}{\Delta V}$, parameterizes the response of the reaction to a change in ambient pressure or temperature. Divariant reactions such as those associated with the seismic discontinuities at 410 and 660 km [Jeanloz and Thompson, 1983] $(Mg,Fe)_2SiO_4$ (α) = $(Mg,Fe)_2SiO_4$ (β) (410 km), $(Mg,Fe)_2SiO_4$ (γ) = $(Mg,Fe)O$ + $(Mg,Fe)SiO_3$ (olivine (γ) = magnesiowüstite + perovskite, 660 km) involve an additional parameter, the width of the two phase loop where products and reactants coexist. For such a reaction, a Clapeyron slope is undefined because the precondition of constant phase composition in the Clausius-Clapeyron relation is violated.

To illustrate the dependence of the two phase loop on thermodynamic properties, we take the $\alpha \rightarrow \beta$ polymorphic reaction in olivine. Consider the variation in composition of α and β as pressure varies holding temperature fixed, analogous to one of the *T=constant* planes in Figure 1. At equilibrium, the chemical potential μ of each component must be equal in all phases. Choosing the Mg_2SiO_4 component in α and β,

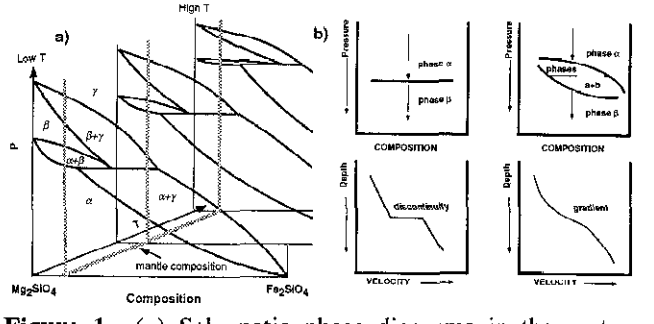

Figure 1. (*a*) Schematic phase diagrams in the system Mg_2SiO_4 – Fe_2SiO_4 showing pressure, temperature and compositional dependence. One- and two-phase fields are labeled α (olivine), β (modified-spinel) and γ (spinel). Gray line marks plane of mantle composition. With increasing temperature, the two phase α+β field shifts to higher pressures and greater depths but thins. (*b*, after Bina and Wood [1987]) Schematic velocity profile through one of the T=const planes of the phase diagram (*right*). The increase in pressure with depth raises velocities above and below the transition region, but in it the gradient changes as the volumetric proportions of the α and β phases change. In pure Mg_2SiO_4, the profile would be discontinuous (*left*).

[1]Geology Department, University of Bristol, Wills Memorial Building, Queens Road, Bristol BS8 1RJ, UK

[2]Dept. of Geological Sciences, Locy Hall, Northwestern University, Evanston IL 60208, USA

Paper number 94GL02341
0094-8534/94/94GL-02341$03.00

$$\mu^{\alpha}_{Mg_2SiO_4} = \mu^{\beta}_{Mg_2SiO_4} \text{ , or } \quad \mu^{\alpha} = \mu^{\beta} \tag{1}$$

for brevity. For any component, $\mu = \mu^0 + RT\ln a \approx \mu^0 + nRT\ln x$, where μ^0 is a standard state μ taken as the pure phase at the pressure and temperature of interest, and assuming the solid solutions in α and β to be ideal ($a \approx x$; x is the component mole fraction in the phase) with mixing on n sites. Thus, using $(\partial\mu/\partial P)_T = V$,

$$\begin{aligned} 0 &= (\partial\mu^{\alpha}/\partial P)_T - (\partial\mu^{\beta}/\partial P)_T \\ &= (\partial\mu^{0,\alpha}/\partial P)_T + nRT(\partial\ln x^{\alpha}/\partial P)_T \\ &\quad - (\partial\mu^{0,\beta}/\partial P)_T - nRT(\partial\ln x^{\beta}/\partial P)_T \\ &= (V^{\alpha} - V^{\beta}) + nRT\left[(\partial\ln x^{\alpha}/\partial P)_T - (\partial\ln x^{\beta}/\partial P)_T\right]. \end{aligned} \tag{2}$$

The locus of points describing the two phase loop is therefore

$$(\partial\ln x^{\alpha}/\partial P)_T = \Delta V/(nRT) + (\partial\ln x^{\beta}/\partial P)_T \quad , \tag{3}$$

revealing that the loop's shape derives from the phases' relative volumetric properties. In reality, these relations are more involved because the activity a depends in a more complex fashion on the compositions x^{α} and x^{β} and contributes further terms to (2) and (3). These activity-composition relations are difficult to constrain experimentally [Wood, 1990], but most recent solid solution models prescribe a thinning of the loop at higher temperatures (Fig. 1a). Even though this parameterization is the simplest thermodynamically, the compositions of the coexisting phases vary in a nonlinear fashion. In turn, this implies a decidedly nonlinear variation of elastic properties through the divariant region.

Frequency Dependence

Clearly, thermodynamic properties govern the morphology of two phase loops. Consider the conditions in the earth's interior near a seismic discontinuity, which are probably roughly adiabatic. Through this or any other region, a P-T trajectory may be calculated with an adiabat initiated at some temperature T_o, $T = T(z,T_o)$. As one progresses along the adiabat downwards through the phase transformation, the P, T conditions progress upwards and towards the rear of Fig. 1a, traversing the two phase $\alpha+\beta$ loop, whose seismic expression is schematically shown in Figure 1b. The consequences of a seismic wave interacting with the gradient depend upon its frequency. Two aspects are of interest here: (1) the amplitudes of the wave conversions and reflections from the gradient and (2) the delay, or time lag, between incidence and emission of each of these waves.

Of these aspects, the most extensively explored has been the amplitude dependence on frequency, or equivalently, gradient zone thickness [Richards, 1972; Lees et al., 1983; Bock and Ha, 1984; Davis et al., 1989]. A rule of thumb is that a gradient is visible to a seismic wave if a significant change in elastic properties occurs within a quarter-wavelength [Richards, 1972]. Thus short period visibility implies sharp gradients approximating discontinuities [Benz and Vidale, 1993], whereas gentle gradients may be observed at long periods [Shearer, 1990; 1991].

The time lag is of interest because the depth to the gradient zone or discontinuity is computed from it. Suppose that the depth to such a region is derived by measuring the time lag between a bottomside reflection and a surface reflected phase such as SS (e.g., Shearer [1991]). At short periods, the discontinuity depth would appear to be at the base of the discontinuity, but at long periods it may appear to be displaced upwards on account of the lag brought about by the longer interaction time. Thus the apparent depth of a gradient zone can vary with frequency.

Despite being gradient zones, the features at 410 and 660 km are called discontinuities. A meaning may be assigned to this apparent inconsistency if it is understood that the gradient is being assigned the depth observationally equivalent to a first order discontinuity. A frequency dependence is implicit in this definition. Similarly, a "seismic Clapeyron slope" for a discontinuity may be defined, which is its displacement in depth in response to a given thermal perturbation. This is also frequency dependent, but it otherwise depends only on thermodynamic properties.

Examples

To illustrate these concepts, we compute the reflection coefficient and time lag associated with a bottomside reflection from a seismic discontinuity produced by the olivine $\alpha \rightarrow \beta$ transformation. Given T_o defining an adiabat, we compute the phase assemblages in a pure olivine mantle of composition $(Mg_{0.9},Fe_{0.1})SiO_4$, and the corresponding density and seismic velocity profiles, between 300 and 500 km depth using a free energy minimization technique [Bina and Wood, 1987], thermodynamic data from Fei et al. [1991], and thermoelastic data from Bina and Helffrich [1992]. Each derived V_P, V_S, and ρ profile is scaled to mantle mineralogy by fitting the adiabatic portions above and below the transition gradient to the IASP91 velocity profile [Kennett and Engdahl, 1991]. This yields a velocity profile under the assumption that only the olivine volume fraction transforms and the remainder is inert. We compute profiles along a 1350°C mantle adiabat initiated at 100 km depth as well as along two adiabats ±400°C, a temperature range encompassing both mantle plume excess temperatures and cool subducted slabs and facilitating the computation of finite-difference derivatives. Figure 2 shows the frequency dependent underside P reflection coefficients computed using a Haskell propagator methodology [Aki and Richards, 1980]. At the 0.5-1 Hz (1-2 s period) and ~18° incidence angle appropriate for $P'_{410}P'$, the warm and cold adiabats' reflectivity varies by a factor of between 2-4, simply due to the broadening of the transition with temperature (Fig. 1). More dramatic variations are possible with different solid solution parameters. Bina and Wood's [1987] olivine solid models give thinner gradients (6-16 km in the ±400° range explored), equivalent reflectivity variation at 0.5-1 Hz but a factor of 12 variation at 1.2-1.5 Hz. In both cases the variation in reflectivity is greater at higher frequencies, illustrating the greater sensitivity of short period observations to gradient zone thickness.

We also compute reflected pulse time lags for these same gradient zones at two frequencies, 0.2 and 0.05 Hz (5 and 20 s period), by propagating an SH-polarized pulse upwards through the gradient zone and measuring the time lag between pulse minima. The lag may be converted to an effective first-order discontinuity depth by integrating through the velocity profiles and finding the depth where the two-way travel time matches the lag. As may be seen in Figure 3, there is a frequency dependence to the pulse minima separation, as well as

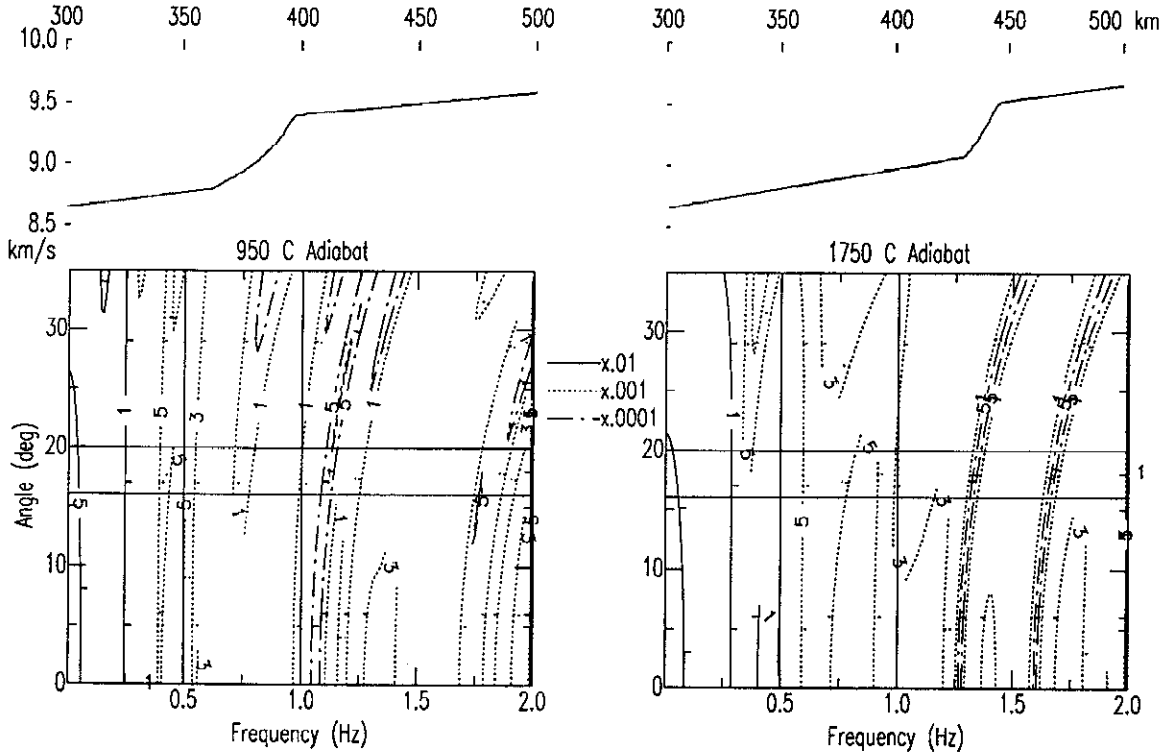

Figure 2. Displacement amplitude P reflection coefficients computed for α+β two-phase gradient zones for 950°C and 1750°C profiles. P velocity profiles shown at top of panels. Contours illustrate dependence of underside reflection coefficient on incidence angle and frequency, with the range relevant for $P'_{410}P'$ delimited by the lines (~18° and 0.5-1 Hz). Between 950°C and 1750°C the reflection coefficient varies by a factor of 2-4, potentially rendering the transformation invisible in the mantle when elevated to lower pressures by cooler temperatures. Conversely, the discontinuity sharpens and deepens at higher temperatures.

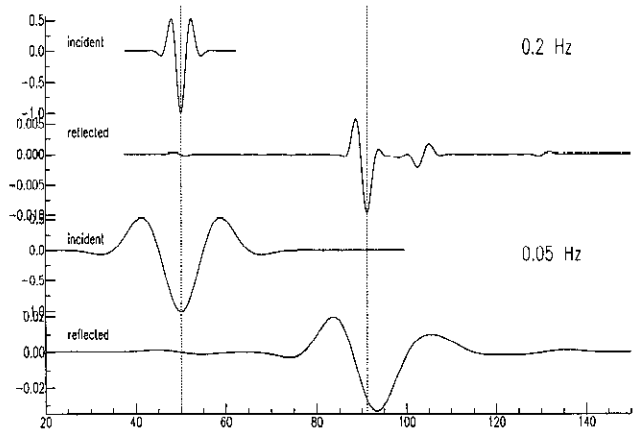

Figure 3. Synthetic seismograms computed through 950°C velocity profile (Fig. 2) of underside SH reflection from the gradient zone at vertical incidence. The pulses have dominant frequencies of 0.2 and 0.05 Hz. Incident pulse minima are aligned on the vertical marker at left. An inferred first-order discontinuity depth may be obtained from the time lag between incidence and reflection. Marker at right shows the 0.05 Hz minimum displaced from that at 0.2 Hz, illustrating the frequency dependence of the time lag, and hence the inferred discontinuity depth.

waveform distortion stemming from energy reflected from both ends of the gradient zone, leading to a frequency dependence to the depth of the equivalent first-order discontinuity. We derive a seismic Clapeyron slope $dP/dT = dP/dz \times dz/dT$ using the discontinuity depths derived from the 950°C and 1750°C profile synthetics. Here dP/dz is the change in pressure with depth z (~100/3 MPa km^{-1} in the Earth's upper mantle), and dz/dT is the discontinuity depth change from a change in temperature. At 0.2 Hz, the seismic dP/dT is 2.04 MPa K^{-1}, whereas at 0.05 Hz it is 2.12 MPa K^{-1}. In the 950°C profile the discontinuity depth inferred at 0.2 Hz is 6.5 km deeper than at 0.05 Hz.

Discussion and Conclusions

The variation with temperature of the gradient zone thickness associated with the olivine α→β transformation has frequency dependent consequences, one of which is variability of the gradient's visibility to seismic waves. Underside P reflectivity changes by factors of 2-4 in the 0.5-1.0 Hz band among the profiles we compute and is comparable to those found for focusing by discontinuity topography [Davis et al., 1989; Neele and Snieder, 1992] but depends in detail on mineral volume and solid solution parameters. The gradient zones will be less visible at shorter periods when deflected upwards by cooler mantle temperatures. On this account, depths to the 410 derived from short period observations [Vidale and Benz,

1992; Benz and Vidale, 1993] will have less apparent variability because the extreme deflections by cooler temperatures will be undetectable [Bina and Helffrich, 1994]. In contrast, the full depth variability would be visible in a transformation that remained sharp at all temperatures, as the transformation associated with the 660 appears to be [Wood, 1990; Fei et al., 1991]. This phenomenon also suggests an explanation for the more consistently observed $P'_{660}P'$ as compared to $P'_{410}P'$ [Nakanishi, 1988; Davis et al., 1989].

The distinction we have drawn between the thermodynamic and seismic Clapeyron slopes is not merely pedagogical. The thermodynamic Clapeyron slope estimated from Fei et al.'s [1991] model for Mg_2SiO_4, the nearest end-member to olivine of mantle composition, is ~2.5 MPa K^{-1}, whereas the seismic slopes we compute are uniformly and significantly smaller by 15-18%. Thus, there are quantitative grounds for treating thermodynamically derived Clapeyron slopes with caution when interpreting seismological observations. For example, an observed 410 deflection of 15 km would suggest between 200 and 245°C temperature variation depending upon whether a short period seismic or a thermodynamic slope is used, a bias larger than the variability in mantle plume temperatures estimated geochemically [Schilling, 1991].

The weak frequency dependence of the seismic Clapeyron slope computed here stems from a correspondingly weak temperature dependence of the two phase loop morphology in the mineralogic model. Where it is stronger, a more striking frequency dependence to the slope results. The uncertainties in the thermodynamic parameters governing the olivine $\alpha \rightarrow \beta$ transition encompass a range of loop morphologies and thermal dependencies. Clearly, conflicting estimates of discontinuity depths, topography, and thermal state can arise if they are neglected.

Acknowledgements. We thank H. Paulssen, P. Richards, and two anonymous reviewers for their constructive criticisms, J. Vidale for preprints and A. Navrotsky and P. Shearer for helpful discussions. UK NERC grant GR9/933'A' to G. H. supported part of this work, while both the NSF (EAR-9158594) and the Petroleum Research Fund of the American Chemical Society (25115-G8) supported C. R. B.

References

Aki, K., and P. G. Richards, *Quantitative Seismology (vol. 1),* 557pp, Freeman, New York, 1980.

Benz, H., and J. Vidale, Sharpness of upper-mantle discontinuities determined from high-frequency reflections, *Nature, 365,* 147–150, 1993.

Bina, C. R., and G. R. Helffrich, Calculation of elastic properties from thermodynamic equation of state principles, *Ann. Rev. Earth Planet. Sci., 20,* 527–552, 1992.

Bina, C. R., and G. Helffrich, Phase transition Clapeyron slopes and transition zone seismic discontinuity topography, *J. Geophys. Res., (in press),* 1994.

Bina, C. R., and B. J. Wood, The olivine-spinel transitions: Experimental and thermodynamic constraints and implications for the nature of the 400 km seismic discontinuity, *J. Geophys. Res., 92,* 4853–4866, 1987.

Bock, G., and J. Ha, Short-period S-P conversion in the mantle at a depth near 700 km, *Geophys. J. R. astron. Soc., 77,* 593–615, 1984.

Davis, J. P., R. Kind, and I. S. Sacks, Precursors to PP' re-examined using broad-band data, *Geophys. J. Int., 99,* 594–604, 1989.

Fei, Y., H.-K. Mao, and B. O. Mysen, Experimental determination of element partitioning and calculation of phase relations in the MgO-FeO-SiO_2 system at high pressure and high temperature, *J. Geophys. Res., 96,* 2157–2169, 1991.

Jeanloz, R., and A. Thompson, Phase transitions and mantle discontinuities, *Rev. Geophys. Space Phys., 21,* 51–74, 1983.

Katsura, T., and E. Ito, The system Mg2SiO4-Fe2SiO4 at high pressures and temperatures: Precise determination of stabilities of oliving, modified spinel and spinel, *J. Geophys. Res., 94,* 15,663–15,670, 1989.

Kennett, B. L. N., and E. R. Engdahl, Traveltimes for global earthquake location and phase identification, *Geophys. J. Int., 105,* 429–465, 1991.

Lees, A. C., M. S. T. Bukowinski, and R. Jeanloz, Reflection properties of phase transition and compositional change models of the 670-km discontinuity, *J. Geophys. Res., 88,* 8145–8159, 1983.

Nakanishi, I., Reflections of PP' from upper mantle discontinuities beneath the Mid-Atlantic Ridge, *Geophys. J. Int., 93,* 335–346, 1988.

Neele, F., and R. Snieder, Topography of the 400 km discontinuity from observations of long-period $P_{410}P$ phases, *Geophys. J. Int., 109,* 670–682, 1992.

Richards, P. G., Seismic waves reflected from velocity gradient anomalies within the Earth's upper mantle, *Z. Geophys., 38,* 517–527, 1972.

Schilling, J.-G., Fluxes and excess temperatures of mantle plumes inferred from their interaction with migrating mid-ocean ridges, *Nature, 352,* 397–403, 1991.

Shearer, P., Seismic imaging of upper-mantle structure with new evidence for a 520-km discontinuity, *Nature, 344,* 121–126, 1990.

Shearer, P., Constraints on upper-mantle discontinuities from observations of long-period reflected and converted phases, *J. Geophys. Res., 96,* 18,147–18,182, 1991.

Vidale, J., and H. Benz, Upper-mantle seismic discontinuities and the thermal structure of subduction zones, *Nature, 356,* 678–683, 1992.

Wood, B. J., Postspinel transformations and the width of the 670-km discontinuity: A comment on "Postspinel transformations in the system Mg_2SiO_4-Fe_2SiO_4 and some geophysical implications" by E. Ito and E. Takahashi, *J. Geophys. Res., 95,* 12,681–12,685, 1990.

G. Helffrich, Geology Department, University of Bristol, Wills Memorial Building, Queens Road, Bristol BS8 1RJ, UK (george@geology.bristol.ac.uk)

Craig R. Bina, Dept. of Geological Sciences, Locy Hall, Northwestern University, Evanston IL 60208, USA

(Received May 27, 1994; revised August 8, 1994; accepted August 19, 1994.)